ARCHIVES OF ELECTRICAL ENGINEERING VOL. X(Y), pp. 1-22 (2027)

This paper has been accepted for publication in the AEE journal. This is the version, which has not been fully edited and content may change prior to final publication.
Citation information: DOI 10.24425/aee.2027.17590

Multi-objective optimal configuration of flexible interconnected power grid topology for new power systems in heavy-load areas

HONG DONG[1]*, YUQUN GAO[1], LIUJUN HU[1], YAHAO CHEN[2], ZEXIN LIU[2]

[1]*Guangzhou Power Supply Bureau of Guangdong Power Grid Co., Ltd.*
Guangzhou 510630, China

[2]*China Energy Engineering Group Guangdong Electric Power Design Institute Co., Ltd.*
Guangzhou 510670, China

*email: {*dh20260117/scutgyyyyq/15116330584}@163.com, {chenyahao/liuzexin}@gedi.com.cn*

Early Access

Abstract: New power systems in heavy-load areas are confronted with threefold pressures, namely insufficient power supply reliability, limited renewable energy accommodation and degraded operational safety. To address the above challenges, a multi-objective optimal configuration method for flexible interconnected power grid topology oriented to heavy-load areas is proposed. Taking the energy storage-based soft open point (E-SOP) as the core regulation and control carrier, the proposed method sets economic indicators as boundary constraints, and takes power balance, node voltage and other indicators as operational constraints. A multi-objective optimal configuration model of flexible interconnected power grid topology is established with three optimization objectives: reliability (minimum load loss after faults), environmental performance (minimum curtailed renewable energy power), and safety (minimum voltage deviation and minimum load rate variance), so as to realize the optimal configuration of new power systems in heavy-load areas. A modified IEEE 33-node test system is adopted to construct a heavy-load area case for verification. The simulation results demonstrate that after optimal configuration via the proposed method, the system can complete fault power transfer within 0.05 s; the power loss is reduced by 88.6%, the comprehensive photovoltaic curtailment rate drops from 22.6% to 4.7%, the minimum node voltage rises from 0.921 p.u. to 0.956 p.u., and the load rate variance is cut down by 88.3%. The results of this study provide a quantitative reference for the planning and retrofit of distribution networks in heavy-load areas with high renewable penetration, although the conclusions are obtained under the specific assumptions of the modified IEEE 33-node case.

Key words: flexible interconnection, heavy-load areas, multi-objective optimization configuration, new power system, power grid topology, smart soft-switching,

Abbreviations
E-SOP: energy storage-based soft open point;
SOP: soft open point;

This paper has been accepted for publication in the AEE journal. This is the version, which has not been fully edited and content may change prior to final publication.
Citation information: DOI 10.24425/aee.2027.17590

DG: distributed generation;
PV: photovoltaic;
SOC: state of charge;
AHP: analytic hierarchy process;
EW: entropy weight;
NSGA-II: non-dominated sorting genetic algorithm II;
O&M: operation and maintenance;
FCL: fault current limiter.

1. Introduction

Driven by the "Dual Carbon" goal, the installed capacity of new energy represented by wind power and photovoltaic power has maintained rapid growth, and a new power system is rapidly taking shape with a fundamental pattern of high-penetration renewable energy integration[1]. As a typical scenario featuring highly concentrated power demand, heavy-load areas are confronted with three core challenges: insufficient power supply reliability, limited new energy accommodation and degraded operational safety[2]. Traditional distribution networks adopt the design principle of "closed-loop design with open-loop operation", without regular power mutual support channels between feeders[3, 4]. Fault recovery relies on switching operations; severe photovoltaic power curtailment occurs when midday peak photovoltaic output coincides with valley load periods. Long-term heavy loading in some transformer districts and light loading in others result in uneven equipment utilization efficiency[5]. Accordingly, it is urgent to investigate an optimal configuration method for new power systems in heavy-load areas to realize regular power mutual support among feeders, millisecond-level load transfer after faults, and coordinated cross-feeder accommodation of new energy[6], so as to systematically resolve the triple dilemmas of "difficult reliable power supply, difficult green energy accommodation and difficult safe operation" existing in heavy-load areas[7].

At present, a number of scholars have carried out relevant research in this field. For instance, Maurya *et al*. [8] adopted the Puma optimization algorithm to conduct optimal planning for various distributed generators (DGs) in radial distribution networks, determining the optimal location and capacity of DGs subject to power flow and voltage constraints. Nevertheless, flexible interconnection devices are not deployed in their scheme, and feeders remain rigidly connected, failing to realize millisecond-level load transfer after faults and thus unable to satisfy the power supply reliability requirements of heavy-load areas. Akbar *et al*. [9] implemented collaborative optimization of distributed generators and fault current limiters, targeting the minimum total system cost with protection coordination as the primary constraint. However, this single-objective method prioritizes economic performance without taking new energy accommodation and operational safety into account, which restricts the comprehensive operational benefits under high-penetration photovoltaic integration. Zhang *et al*. [10] carried out optimal configuration of battery energy storage systems. The fast charge-discharge response

Early Access

This paper has been accepted for publication in the AEE journal. This is the version, which has not been fully edited and content may change prior to final publication.
Citation information: DOI 10.24425/aee.2027.17590

of energy storage provides active power support to enhance voltage and frequency stability under weak grid conditions. Yet the regulation range of energy storage is limited by its rated capacity, and it only supports local single-point regulation without global cross-feeder power mutual support capacity, leading to limited suppression effect on photovoltaic curtailment. Prasad et al. [11] adopted a stochastic gradient control algorithm to adjust the reactive power injection of photovoltaic inverters in real time, taking voltage total harmonic distortion and three-phase unbalance factor as indicators to improve power quality. However, this method only addresses power quality issues, cannot realize cross-feeder transfer of active power, and ignores the demand for load transfer under fault conditions.

Flexible interconnection devices rely on three regulation mechanisms: accurate active power transfer, dynamic reactive power compensation and rapid post-fault load transfer[12]. They can effectively tackle core problems including insufficient power supply reliability, restricted new energy accommodation and deteriorated operational safety in heavy-load areas, and have become a prominent research focus in the field of new power systems[13]. Their millisecond-level response speed overcomes the drawback of minute-level switching operations of traditional tie switches; their continuously adjustable active power transmission capability breaks the rigid barrier of "open-loop operation" between feeders; and their dynamic reactive power compensation capacity provides a flexible solution for voltage violation problems[14].

In addition to optimizing physical power grid equipment, the integration of advanced data-driven and predictive technologies is also crucial for the safe and economical operation of new power systems. For example, literature has explored carbon aware machine learning and joint optimization frameworks to improve energy efficiency in data centers [15]. These studies indicate that accurate prediction of renewable energy production and load demand is the foundation for alleviating the uncertainty faced by heavy load areas. In addition, the economic regulation and load forecasting of the distribution network have also attracted widespread attention. Reference [16] compared statistical methods and artificial neural networks for power load forecasting. Although these studies provide valuable tools for economic dispatch and load forecasting, they mainly focus on predicting operational levels or economic incentives. They cannot solve topology level reconstruction problems, nor can they directly provide millisecond level fault recovery and physical cross feeder power transmission capabilities required for large-scale renewable energy accommodation in overloaded areas.

In this paper, the “flexible interconnected power grid topology” is defined as a reconfigurable distribution-network topology in which feeders are connected by flexible interconnection devices (e.g., E-SOP) rather than rigid tie switches. Its vertices are the feeder nodes/substations, and its edges are the flexible interconnection branches whose active and reactive power flows can be continuously and rapidly regulated. Therefore, the topology is not a fixed switching state but a set of controllable cross-feeder power-transfer relationships determined by the siting, sizing and operating strategy of E-SOP devices. Therefore, this paper proposes a multi-objective optimal configuration method for flexible interconnected power grid topology oriented to new power systems in heavy-load areas. The main contributions and significance are as follows:

Early Access

This paper has been accepted for publication in the AEE journal. This is the version, which has not been fully edited and content may change prior to final publication.
Citation information: DOI 10.24425/aee.2027.17590

1) a flexible interconnection topology model based on the E-SOP is established, which simultaneously represents active power transfer, reactive power compensation and fault transfer;

2) a multi-objective configuration model considering reliability, environmental performance and safety is formulated, with economic feasibility as a boundary constraint rather than a parallel objective, which reflects the engineering logic of "technical optimality within a limited investment"; and

3) a modified IEEE 33-node heavy-load case is constructed to quantify the coordinated improvement of reliability, renewable energy accommodation and operational safety, providing a reference for the planning and retrofit of distribution networks with high renewable penetration.

2. Multi-objective optimal configuration model of flexible interconnected grid topology

2.1. Mechanism and key elements of flexible interconnection grid topology optimization

New power systems in heavy-load regions face the triple challenges of power supply reliability, renewable energy integration, and operational safety [17]. Flexible interconnection devices can effectively address these challenges through three control mechanisms: precise active power transfer, dynamic reactive power compensation, and rapid power supply switching after a fault [18]. The decision variables optimized in the proposed method are:

(i) the installation location and capacity of each E-SOP port, i.e., the binary siting variable and the continuous capacity variable of the E-SOP;

(ii) the active power transfer and reactive power of each E-SOP port at each time slot tt;

(iii) the charging/discharging power of the energy storage units; and

(iv) the branch connection of the reconfigurable network.

The objective functions and constraints given in Sections 2.2–2.4 are all formulated with respect to these variables. The three control mechanisms are as follows:

1) Active power transfer mechanism

Suppose that in a heavy-load area, the flexible interconnection device E-SOP in the new power system connects feeder *i* to feeder *j*. Then, the active power balance satisfied during the time interval *t* is:

$$P_{\mathrm{SOP},i,t} + P_{\mathrm{SOP},j,t} + P_{\mathrm{SOP},t}^{\mathrm{loss}} = 0, \tag{1}$$

where $P_{\mathrm{SOP},i,t}$ and $P_{\mathrm{SOP},j,t}$ are the active power injected into feeders i and j, respectively; $P_{\mathrm{SOP},t}^{\mathrm{loss}}$ is the active power loss of the E-SOP, typically taken as 2%–3% of the transmitted power.

2) Reactive power compensation mechanism

Each port of the E-SOP flexible interconnection device independently regulates reactive power, and the port p' must satisfy the following capacity constraint:

$$\sqrt{P_{\mathrm{SOP},\,p',t}^2 + Q_{\mathrm{SOP},\,p',t}^2} \le S_{\mathrm{SOP},\,p'}, \tag{2}$$

Early Access

This paper has been accepted for publication in the AEE journal. This is the version, which has not been fully edited and content may change prior to final publication.
Citation information: DOI 10.24425/aee.2027.17590

where $Q^2_{\mathrm{SOP},\,p',t}$ represents the reactive power at E-SOP port p'; and $S_{\mathrm{SOP},\,p'}$ represents the capacity of E-SOP port p'.

3) Fault power transfer mechanism

The power transfer capability coefficient of the E-SOP flexible interconnection device under a fault scenario is defined as:

$$\gamma_f = \frac{P_{\mathrm{transfer},f}}{P^{\mathrm{noSOP}}_{\mathrm{loss},f}}, \tag{3}$$

where $P_{\mathrm{transfer},f}$ is the load power successfully transferred when the E-SOP participates under a fault scenario, and $P^{\mathrm{noSOP}}_{\mathrm{loss},f}$ is the lost load power when the E-SOP does not participate.

Based on the above three control mechanisms, the multi-objective optimization of flexible interconnection grid topologies for new power systems in heavy-load regions requires decisions on the following core elements: the port capacity $S_{\mathrm{SOP},\,p'}$ of the flexible interconnection device E-SOP and the interconnection line state vector α^{line}. Economic feasibility serves as a boundary constraint and is not included in the multi-objective optimization to ensure that the designed optimization scheme is feasible within the investment limit. Sections 2.2 through 2.4 below establish specific optimization models based on this approach.

Early Access

2.2. Economic boundary constraints for topological optimization of flexible interconnected power grids

Before the optimization, economic boundary constraints are first established as hard criteria for screening optimization solutions. The total investment constraint for the optimization is as follows:

$$C_{\mathrm{total}} = \sum_{k=1}^{N_{\mathrm{SOP}}}\left(c_{\mathrm{SOP}} \cdot S_{\mathrm{SOP},k}\right) + \sum_{l=1}^{N_{\mathrm{line}}}(c_{\mathrm{line}} \cdot \alpha_l) \le C_{\max}, \tag{4}$$

where: N_{SOP} is the number of candidate flexible interconnection devices to be installed; $S_{\mathrm{SOP},k}$ is the capacity of the E-SOPs numbered k; c_{SOP} is the investment cost per unit of capacity; N_{line} is the number of candidate new or retrofitted lines; α_l is a 0–1 decision variable indicating whether the l-th interconnection line is closed; c_{line} is the investment cost per line; and $C_{\max}$ is the upper limit on total investment. This constraint ensures that all optimization schemes remain within an acceptable investment range.

2.3. Multi-objective optimization model for flexible interconnected grid topology

Based on the analysis of the E-SOP control mechanism for flexible interconnection devices in Section 2.1 and the economic boundary constraints in Section 2.2, this section establishes three objective functions: reliability, environmental sustainability, and safety. These three objectives characterize the optimization requirements for flexible interconnection grids in heavy-load regions from different perspectives: reliability reflects the new power system's ability to withstand faults; environmental sustainability reflects the level of renewable energy integration; and safety characterizes the balance between voltage quality and equipment utilization [19]. The specific objectives are as follows:

This paper has been accepted for publication in the AEE journal. This is the version, which has not been fully edited and content may change prior to final publication.
Citation information: DOI 10.24425/aee.2027.17590

1. Reliability objective: minimize load loss

Heavy-load regions have extremely stringent requirements for power supply reliability, and the ability to transfer load following a fault is a core indicator for measuring the reliability of the new power system in such regions. Traditional interconnection switches have long switching times, making it difficult to meet the requirements for continuous power supply to critical loads [20]; in contrast, the flexible interconnection device E-SOP can complete fault isolation and load transfer within milliseconds, significantly reducing the amount of lost load. Therefore, this section aims to minimize the power loss in the new power system under a set of anticipated fault scenarios in heavy-load regions, directly reflecting the improvement in power supply reliability achieved by the flexible interconnection topology. Let Φ_{fault} denote the set of fault scenarios in heavy-load regions; the power loss of the system under each fault is defined as:

$$P_{\text{loss},f} = \sum_{i=1}^{N_{\text{node}}} (1 - \beta_{i,f}) \lambda_{i,f} P_{L',i}. \tag{5}$$

In the equation, $f \in \Phi_{\text{fault}}$ is the index of the heavy-load area fault scenario; N_{node} is the total number of load connection nodes; $P_{L',i}$ is the active power of the load at node i; $\beta_{i,f}$ is a 0–1 variable indicating whether power supply to node *i* is restored under fault scenario *f* (1 indicates restoration); $\lambda_{i,f}$ is the overload shedding ratio during load transfer, with a value in the range [0, 1]. The reliability objective function is to minimize the average load loss across all fault scenarios:

$$\min E_1 = \sum_{f=1}^{N_{\text{fault}}} P_{\text{loss},f} / N_{\text{fault}}, \tag{6}$$

where N_{fault} is the total number of anticipated faults in heavy-load areas. This objective leverages the rapid power control capability of the flexible interconnection device E-SOP to achieve millisecond-level load transfer after a fault, thereby meeting the core requirement for high power supply reliability in heavy-load areas. It should be noted that Eq. (6) is intrinsically linked to the load transfer capability coefficient γ_f in Eq. (3)—the smaller the system's lost load power $P_{\text{loss},f}$ during a fault, the closer γ_f is to 1, indicating a more significant improvement in the reliability of the flexible interconnection topology.

2. Environmental objectives: maximizing renewable energy integration

A core characteristic of the new power system is the high proportion of renewable energy integration. heavy-load areas typically possess the dual attributes of both abundant renewable energy and dense loads; however, traditional distribution grids lack power transfer channels across feeders, leading to significant curtailment of solar power during midday when peak photovoltaic output overlaps with off-peak load periods [21].The active power transfer capability of the flexible interconnection device E-SOP can transfer surplus renewable energy power from lightly loaded feeders to heavily loaded feeders or energy storage devices, thereby improving the system's on-site renewable energy absorption rate. This section aims to minimize daily curtailed wind and solar power, demonstrating the contribution of the flexible interconnection topology to low-carbon and environmental protection goals.

Define the curtailed wind and solar power for distribution substation *i* during time slot *t* as:

Early Access

This paper has been accepted for publication in the AEE journal. This is the version, which has not been fully edited and content may change prior to final publication.
Citation information: DOI 10.24425/aee.2027.17590

$$\Delta P_{\mathrm{DG},i,t} = P_{\mathrm{DG},i,t}^{\max} - P_{\mathrm{DG},i,t}^{\mathrm{con}}, \tag{7}$$

where $P_{\mathrm{DG},i,t}^{\max}$ is the maximum available output of distributed generation (PV and wind power) in distribution substation *i* during time slot *t*; and $P_{\mathrm{DG},i,t}^{\mathrm{con}}$ is the actual active power consumed. The environmental objective is to minimize the system's total daily curtailed wind and solar power:

$$\min E_2 = \sum_{t=1}^{24} \sum_{i=1}^{N_{\mathrm{arca}}} \Delta P_{\mathrm{DG},i,t} \Delta t, \tag{8}$$

where N_{arca} is the total number of distribution zones and Δt is the dispatch time slot interval (set to 1 hour). This objective is achieved by transferring surplus renewable energy power to heavy-load areas or energy storage facilities via the flexible interconnection device E-SOP, thereby reflecting the low-carbon and environmental requirements of the new power system. It is worth noting that the active power transfer mechanism in Eq. (8) directly corresponds to that in Eq. (1)—the reasonable control of $P_{\mathrm{SOP},i,t}$ is key to minimizing $\Delta P_{\mathrm{DG},i,t}$.

3. Safety objectives: voltage deviation and load balancing

Under the dual influence of fluctuations in renewable energy output and alternating peak and off-peak loads, heavy-load areas are prone to voltage out-of-limit conditions and uneven feeder load distribution. Voltage out-of-limit conditions can affect equipment lifespan and the user's power consumption experience; in severe cases, they may trigger protective actions, leading to cascading failures. Uneven load distribution, on the other hand, results in some equipment operating under long-term heavy loads while others remain underlight loads, thereby reducing overall asset utilization [22]. The reactive power compensation capability of the flexible interconnection device E-SOP can suppress voltage fluctuations, while its active power transfer capability can balance the power distribution across feeders. This section breaks down the safety objective into two sub-objectives—voltage deviation and load balancing—which are modeled as follows:

1) Minimization of voltage deviation

Voltage deviation is a fundamental indicator for measuring power quality in the new power system [23]. The flexible interconnection device E-SOP dynamically adjusts reactive power output through the VdcQ control mode, thereby maintaining node voltage within permissible limits when renewable energy output fluctuates. The full-day average voltage deviation in the new power system is defined as:

$$\min E_{3(1)} = \sum_{t=1}^{24} \sum_{i=1}^{N_{\mathrm{node}}} \left| \left(V_{i,t} - \tilde{V}\right) / \tilde{V} \right| / 24 N_{\mathrm{node}}, \tag{9}$$

where, $V_{i,t}$ is the actual voltage amplitude at node *i* during time slot *t*; and $\tilde{V}$ is the rated voltage. This metric utilizes the reactive power compensation capability of the flexible interconnection device E-SOP (Eq. (2)) to improve voltage distribution and suppress voltage overshoots.

2) Minimizing the variance of the load factor across distribution zones

Load balancing reflects the uniformity of power distribution among different distribution zones. In heavy-load areas, some distribution zones are often overloaded while others are underloaded. The flexible interconnection topology can use the active power transfer capability of the E-SOP (Eq. (1)) to transfer power from overloaded distribution zones to underloaded ones,

Early Access

This paper has been accepted for publication in the AEE journal. This is the version, which has not been fully edited and content may change prior to final publication.
Citation information: DOI 10.24425/aee.2027.17590

thereby reducing the variance of the load factor. The load factor of distribution zone *i* during time slot *t* is defined as:

$$\chi_{i,t} = \frac{P_{T',i,t}}{S_{T',i}\cos\varphi}, \tag{10}$$

where: $P_{T',i,t}$ is the active power on the low-voltage inside of the transformer in substation *i* during time slot *t*; $S_{T',i}$ is the rated capacity of the transformer; and $\cos\varphi$ is the power factor. The variance of the load factor for time slot *t* is:

$$\varepsilon_{\mathrm{SLR},t} = \sum_{i=1}^{N_{\mathrm{arca}}}\left(\chi_{i,t} - \sum_{j=1}^{N_{\mathrm{arca}}}\chi_{j,t}/N_{\mathrm{arca}}\right)^2/N_{\mathrm{arca}}. \tag{11}$$

The safety objective is to minimize the variance of the daily average load factor:

$$\min E_{3(2)} = \frac{\sum_{t=1}^{24}\varepsilon_{\mathrm{SLR},t}}{24}. \tag{12}$$

The two sub-objectives described above characterize system safety from the dimensions of voltage quality (Eq. (9)) and equipment utilization (Eq. (12)), respectively. The two are optimally coordinated through the E-SOP's reactive power compensation and active power transfer capabilities. The comprehensive safety objective is expressed as the weighted sum of the two sub-objectives:

$$\min E_3 = \omega_V \min E_{3(1)} + \omega_\chi \min E_{3(2)}, \tag{13}$$

where ω_V and ω_χ are the weighting coefficients for voltage and load factor, respectively; their sum is 1, and they can be set according to the actual engineering requirements of heavy-load regions—if voltage out-of-limit issues are prominent, ω_V should be increased; if load imbalance is severe, ω_χ should be increased. The weighting coefficients ω_V and ω_χ in Eq. (13) are determined by a combined subjective–objective method to avoid arbitrary manual tuning. First, the two sub-objectives $E_{3(1)}$ and $E_{3(2)}$ are normalized by their respective values under the base case to eliminate dimension and magnitude differences. Then, the entropy weight method is used to obtain the objective weights ω_i^{EW} based on the dispersion degree of the candidate solutions, and the analytic hierarchy process (AHP) is used to obtain the subjective weights ω_i^{AHP} according to the engineering priority of voltage quality and equipment utilization in heavy-load areas.

The final weight is $\omega_i = \alpha\omega_i^{\mathrm{EW}} + (1-\alpha)\omega_i^{\mathrm{AHP}}$, with $\alpha = 0.5$. In this paper, the resulting weights are $\omega_V = 0.6$ and $\omega_\chi = 0.4$, reflecting that voltage out-of-limit issues are more prominent during the evening peak in the tested heavy-load case. A sensitivity check with ±20% perturbation of ω_V shows that the minimum node voltage and load-rate variance change by less than 3%, indicating that the safety optimization result is robust to the weight setting.

Taking into account the multiple objective functions described above, the multi-objective optimization configuration model proposed in this paper for flexible interconnection grid topologies in new power systems for heavy-load areas can be summarized as follows:

$$\min E = [E_1, E_2, E_3]^T, \tag{14}$$

Early Access

This paper has been accepted for publication in the AEE journal. This is the version, which has not been fully edited and content may change prior to final publication.
Citation information: DOI 10.24425/aee.2027.17590

where: E_1 represents the amount of lost load (reliability objective), E_2 represents the amount of curtailed wind and solar power (environmental objective), and E_3 represents the comprehensive safety indicator (voltage deviation and variance of load factor).These three objectives characterize the optimization requirements for flexible interconnected grid topologies in new power systems within heavy-load regions from different dimensions: reliability ensures continuous and uninterrupted power supply; environmental sustainability promotes the efficient integration of renewable energy; and safety maintains voltage quality and equipment balance. Together, they form a comprehensive evaluation system for new power systems, providing the objective basis for subsequent optimization under given constraints.

2.4. Operational constraints for multi-objective optimization of flexible interconnected grid topologies

Based on the multi-objective optimization configuration shown in Eq. (14), a series of constraints must be imposed to ensure the physical feasibility and operational safety of the optimized configuration scheme. In addition to the economic boundary constraints discussed in Section 2.2, the new power system in heavy-load regions must also satisfy the following operational constraints. These constraints form a complete closed-loop system with the E-SOP control mechanism for flexible interconnection devices described in Section 2.1 and the multi-objective functions outlined in Section 2.3—the mechanism analysis provides the basis for control, the objective functions define the optimization direction, and the constraints delimit the feasible region. The specific constraints are as follows:

1) Power balance constraint

Power balance is a fundamental prerequisite for the stable operation of the new power system. Based on the active power transfer mechanism of the E-SOP described in Section 2.1, and taking into account the output of distributed generation sources, load demand, energy storage charging and discharging, and interconnection line power, the node power balance equation is:

$$P_{\mathrm{SOP},i,t} + P_{\mathrm{DG},i,t}^{\mathrm{con}} = P_{L',i,t} + P_{\mathrm{ESS},i,t} + \sum_{j=1}^{\Omega_i} P_{\mathrm{line},ij,t}, \tag{15}$$

where: $P_{\mathrm{ESS},i,t}$ represents the energy storage charging/discharging power; Ω_i represents the set of substations interconnected with substation i; and $P_{\mathrm{line},ij,t}$ represents the transmission power over the interconnection line. This constraint ensures that the power injected into and flowing out of each node remains in balance at any given time.

2) Node voltage constraints

To ensure power quality and equipment safety, node voltages must be maintained within permissible limits. In conjunction with the voltage deviation targets in Section 2.3, the voltage amplitude constraints are:

$$V_{\min} \le V_{i,t} \le V_{\max}, \tag{16}$$

where $V_{\max}$ and $V_{\min}$ represent the upper and lower voltage limits, respectively.

3) Branch capacity constraints

Early Access

This paper has been accepted for publication in the AEE journal. This is the version, which has not been fully edited and content may change prior to final publication.
Citation information: DOI 10.24425/aee.2027.17590

To prevent faults caused by line overloads, branch current must not exceed its thermal stability limit:

$$I_{ij,t} \le I_{ij,\max}, \tag{17}$$

where $I_{ij,t}$ is the RMS value of the current in branch ij and $I_{ij,\max}$ is the maximum allowable current.

4) E-SOP operational constraints

Each port of the E-SOP flexible interconnection device must satisfy capacity constraints and multi-port active power balance to ensure the safe operation of the device itself. The port capacity constraint is shown in Eq. (2), and the multi-port active power balance constraint is:

$$\sum_{p'=1}^{N_{p'}} P_{\mathrm{SOP},p',t} + P_{\mathrm{SOP},t}^{\mathrm{loss}} = 0, \tag{18}$$

where $N_{p'}$ is the number of ports. This constraint is consistent with the E-SOP active power transfer mechanism described in Eq. (1) of Section 2.1 and represents the specific implementation of the power balance constraint in Eq. (15) at the E-SOP device level.

5) Energy storage operation constraints

Energy storage systems play a critical role in renewable energy integration (Eq. (8)) and peak shaving and valley filling. The state of charge of the energy storage system must satisfy upper and lower limit constraints, and the charging and discharging power must not exceed the rated value:

$$\begin{cases} S_{\mathrm{SOC},\min} \le S_{\mathrm{SOC},i,t} \le S_{\mathrm{SOC},\max} \\ -P_{\mathrm{ESS},i}^{\max} \le P_{\mathrm{ESS},i,t} \le P_{\mathrm{ESS},i}^{\max} \end{cases}, \tag{19}$$

where: $S_{\mathrm{SOC},i,t}$ is the state of charge of the energy storage system and $P_{\mathrm{ESS},i}^{\max}$ is the maximum charging/discharging power.

6) Radial topology constraints

To ensure the safe operation of the new power system and the feasibility of relay protection coordination, the restructured distribution network must satisfy radial and connectivity constraints:

$$\sum_{ij=1}^{\Omega_{\mathrm{br}}} \delta_{ij} = N_{\mathrm{node}} - N_{\mathrm{sub}}, \tag{20}$$

where: δ_{ij} is a 0–1 variable indicating whether branch j is closed; Ω_{br} is the set of branches; and N_{sub} is the number of power source (substation) nodes. This constraint ensures that the optimized grid topology does not contain loops or isolated islands, thereby complying with the operational standards for distribution grids in heavy-load areas.

In summary, the optimization method developed in this section is strictly centered on four core characteristics: heavy-load areas, new power systems, flexible interconnection grid topologies, and multi-objective optimization. It uses the flexible interconnection device E-SOP as the core control mechanism; by analyzing the three control mechanisms of the E-SOP, it reveals its triple capabilities of active power transfer, reactive power compensation, and fault

Early Access

This paper has been accepted for publication in the AEE journal. This is the version, which has not been fully edited and content may change prior to final publication.
Citation information: DOI 10.24425/aee.2027.17590

transfer supply; using economic feasibility as a boundary constraint to ensure that the optimized configuration scheme is feasible within the investment limit; setting reliability, environmental sustainability, and safety as optimization objectives to respectively address the core needs of heavy-load regions for continuous and uninterrupted power supply, efficient integration of renewable energy, and voltage quality and equipment balance; and using the constraints in Eqs. (5) to (20) to ensure the physical feasibility of the multi-objective optimization configuration scheme. These three objectives are independent yet intrinsically coupled through the control capabilities of the flexible interconnection device E-SOP, collectively forming a comprehensive optimization model for the topological configuration of flexible interconnection grids in new power systems serving heavy-load regions

3. Analysis of experimental results

To verify the effectiveness of the multi-objective optimization method for flexible interconnection grid topology proposed in this paper in actual new power systems of heavy-load regions, this study constructed a new power system based on the modified IEEE 33-node system that reflects the characteristics of heavy-load regions for experimental validation. The heavy-load regions described in the experiments primarily include urban core commercial districts, large industrial parks, and high-density residential communities. These areas exhibit the following typical characteristics: First, high load density, with electricity demand per unit area far exceeding that of ordinary regions; in some service areas, the load factor frequently exceeds the 80% safety threshold during peak hours. Second, a large peak-to-valley difference; influenced by industrial, commercial, and residential electricity consumption patterns, load surges sharply during morning and evening peak hours while plummeting during midday and nighttime, placing high demands on the grid's peak-shaving capacity. Third, there is a high penetration rate of renewable energy. In response to the "dual carbon" goals, distributed photovoltaic (PV) and energy storage systems are typically connected on a large scale within these areas; however, due to the lack of power transfer channels across feeders in traditional distribution grids, significant curtailment of PV generation often occurs when midday PV output peaks coincide with load troughs.

This experimental power system comprises three 10 kV feeders, 33 nodes, and a total load of 7.2 MW (during peak periods), with a PV penetration rate of 45%. It is equipped with two energy-storage-based intelligent soft switches (E-SOPs) serving as flexible interconnection devices, installed at key interconnection points between feeders, with each feeder corresponding to a single service area. The topology of the experimental new power system is shown in Fig. 1.

Early Access

This paper has been accepted for publication in the AEE journal. This is the version, which has not been fully edited and content may change prior to final publication.
Citation information: DOI 10.24425/aee.2027.17590

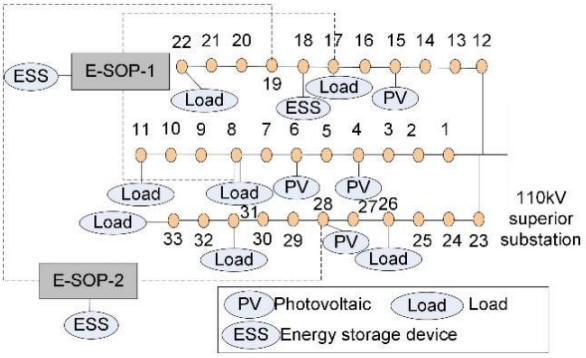

Fig. 1. Topology of the experimental new power system

The experimental power system comprises three 10 kV feeders: Feeder 1 extends from Node 1 to Node 11, Feeder 2 from Node 12 to Node 22, and Feeder 3 from Node 23 to Node 33. The starting nodes of all three feeders (Node 1, Node 12, and Node 23) are connected to the 10 kV busbar of the 110 kV substation. In terms of load and distributed generation configuration, nodes 4, 6, 8, and 11 on Feeder 1 are connected to 120 kW, 500 kW, 200 kW, and 150 kW of photovoltaic generation and load, respectively; Node 15 on feeder 2 is connected to a 400 kW PV system, node 17 to a 320 kW load, node 18 is equipped with a 200 kWh energy storage system, and node 22 to a 180 kW load; node 26 on feeder 3 is connected to a 180 kW load, node 28 to a 600 kW PV system, node 31 to a 220 kW load, and node 33 to a 140 kW load. Regarding the configuration of flexible interconnection devices, the system is equipped with two energy-storage-type smart soft switches (E-SOP): E-SOP-1 connects Node 8 of Feeder 1 to Node 17 of Feeder 2, with a capacity of 800 kVA, and is equipped with Energy Storage Unit 1 (200 kW/400 kWh);E-SOP-2 connects Node 19 on Feeder 2 to Node 28 on Feeder 3, with a capacity of 800 kVA, and is equipped with Energy Storage Unit 2 (200 kW/400 kWh). Each E-SOP operates in PQ-VdcQ control mode to enable active power transfer and reactive power compensation between feeders.

Based on this experimental power system, the optimization effects of the method proposed in this paper are verified below from the three aspects of reliability, environmental friendliness, and safety.

The multi-objective model is solved by the NSGA-II algorithm implemented in MATLAB R2022b with the YALMIP toolbox, where the power-flow and constraint checks are performed by MATPOWER. The population size is 100, the maximum number of generations is 200, the crossover probability is 0.9, the mutation probability is 0.1, and the distribution indices for crossover and mutation are 20 and 20, respectively. The algorithm stops when either the maximum generation is reached or the hypervolume indicator has not improved by more than 10^{-4} over 20 consecutive generations. A Pareto front of 50 non-dominated solutions is obtained, and the compromise solution is selected by the weighted-sum index of Eq. (13).

3.1. Verification of the effect on improving power supply reliability

Early Access

This paper has been accepted for publication in the AEE journal. This is the version, which has not been fully edited and content may change prior to final publication.
Citation information: DOI 10.24425/aee.2027.17590

To verify the effectiveness of the method proposed in this paper in enhancing power supply reliability in heavy-load areas, an N-1 fault scenario was simulated: the outlet circuit breaker of Feeder 2 tripped, causing all nodes 12–22 served by Feeder 2 to lose power. The load restoration performance under two scenarios—a configuration without flexible interconnection (traditional interconnection switch operations) and the optimized configuration proposed in this paper (millisecond-level power transfer via the E-SOP)—was compared, with the results shown in Fig. 2.

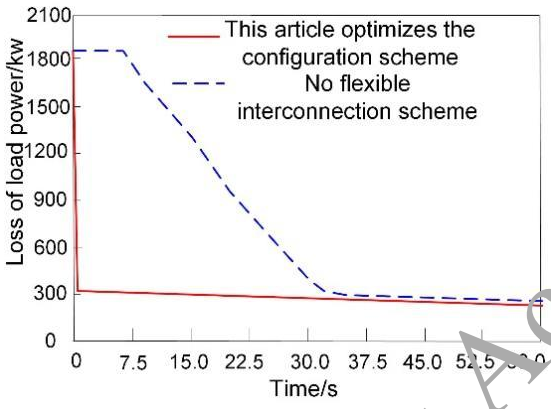

Fig. 2. Comparison of load recovery process of different configuration schemes after fault

Early Access

As shown in Fig. 2, under the non-flexible interconnection scheme, it took 32 seconds after the fault for fault location and switching operations to be completed before the load was gradually restored to 320 kW. During this period, the peak lost load power reached 1 850 kW, with a total power loss of 24.6 kWh; whereas under the optimized configuration described in this paper, the E-SOP completes fault isolation and load transfer within 0.048 s, resulting in a peak power loss of only 320 kW and a total power loss reduced to 2.8 kWh—a reduction of 88.6%.The reason the optimized configuration proposed in this paper achieves such a significant improvement in reliability is as follows: First, the E-SOP employs a millisecond-level response control strategy, enabling detection and action within 0.02–0.05 s after a fault occurs, thereby avoiding the minute-level switching wait times associated with traditional interconnection switches; Second, the E-SOP features continuously adjustable active power transmission capability, enabling precise load transfer from the faulted feeder within capacity constraints and avoiding the need to forcibly shed part of the load due to line overloading, as occurs in traditional solutions; third, the coordinated operation of E-SOP-1 and E-SOP-2 distributes the faulted load from Feeder 2 to Feeders 1 and 3, thereby avoiding the risk of overloading a single transfer path. This demonstrates that the optimized configuration proposed in this paper improves power supply reliability in heavy-load areas through the rapid load transfer and coordinated dispatch of the flexible interconnection device E-SOP.

The load recovery status at each node is shown in Table 1.

This paper has been accepted for publication in the AEE journal. This is the version, which has not been fully edited and content may change prior to final publication.
Citation information: DOI 10.24425/aee.2027.17590

Table 1. Comparison of node load recovery for different configuration schemes after a fault

Node number	Load power/kW	No flexible interconnection		This paper optimizes the configuration	
		Recovery time/s	Complete recovery	Recovery time/s	Complete recovery
12	180	35	Yes	0.046	Yes
15	245	35	Yes	0.046	Yes
18	320	52	Yes	0.046	Yes
20	195	52	Yes	0.046	Yes
22	160	—	No (overload cut-off 30%)	0.046	Yes

The results in Table 1 show that under the optimized configuration scheme proposed in this paper, all nodes completed load recovery within 0.05 s without any overload tripping, verifying the significant role of the flexible interconnection topology in enhancing power supply reliability in heavy-load areas. Specifically: Under the scenario without a flexible interconnection, it took 52 seconds for Node 18 (320 kW) and Node 20 (195 kW) to have power restored; Node 22 (160 kW) had 30% of its load (i.e., 48 kW) shed due to line overload and never fully recovered. The total system power loss reached 1 850 kW, resulting in a prolonged power outage with a wide-ranging impact. However, under the optimized configuration proposed in this paper, E-SOP-1 transfers a portion of the active power from nodes 17 and 18 on Feeder 2 to node 8 on Feeder 1 within 0.046 s, while E-SOP-2 simultaneously transfers active power from nodes 19, 20, and 22 on Feeder 2 to node 26 on Feeder 3. The two transfer channels work in concert to share the load of the faulty feeder, enabling rapid voltage recovery at all nodes following the transfer. All nodes achieved 100% full load restoration without any overload tripping. In comparison, the method described in this paper—through the millisecond-level response of the flexible interconnection device E-SOP and dual-channel coordinated power transfer—not only reduces load restoration time from minutes to milliseconds but also completely eliminates load shedding caused by line overloads, fully meeting the high-reliability requirements for "uninterrupted, loss-free" power supply in heavy-load areas.

Early Access

3.2. Verification of environmental improvement effects

To evaluate the effectiveness of the method in improving the system's environmental performance, an analysis was conducted during a typical peak PV output period (12:00–14:00) to assess the enhancement in the system's renewable energy integration capacity. The PV integration performance and curtailment rates for each feeder were compared between the scenario without a flexible interconnection configuration and the optimized configuration proposed in this paper. The results are shown in Table 2.

Table 2. Comparison of PV consumption of each feeder during midday peak hours

This paper has been accepted for publication in the AEE journal. This is the version, which has not been fully edited and content may change prior to final publication.
Citation information: DOI 10.24425/aee.2027.17590

Feeder	PV maximum available output/kW	Power consumption without flexible interconnection/kW	This paper optimizes the configuration of absorbed power/kW	No flexible interconnection accommodation rate/%	This paper optimizes the allocation of accommodation rate/%
Feeder 1	500	294	481	58.8	96.2
Feeder 2	400	337	380	84.3	95.1
Feeder 3	600	459	569	76.5	94.8
Power system integration	—	—	—	77.4	95.3

As shown in Table 2, under the scheme without flexible interconnection, Feeder 1, due to its relatively low local load, was unable to absorb a large amount of PV power, resulting in an absorption rate of only 58.8% and a curtailment rate of 41.2%; Although Feeders 2 and 3 have larger loads and higher PV absorption rates, the lack of cross-feeder power transfer channels prevents them from absorbing the surplus PV power from Feeder 1, resulting in an overall system absorption rate of only 77.4% and a curtailment rate of 22.6%.Under the optimized configuration proposed in this paper, the E-SOP transfers active power from Feeder 1 to Feeders 2 and 3, increasing the PV absorption rates of the three feeders from 58.8%, 84.3%, and 76.5% to 96.2%, 95.1%, and 94.8%, respectively. and the system's overall solar curtailment rate drops from 22.6% to 4.7%—a reduction of 79.2%—effectively resolving the structural contradiction in heavy-load areas where "feeder lines with high PV concentration lack the capacity to absorb the power, while feeder lines with dense loads have no power available."

Figure 3 shows a comparison of curtailment rates across different time periods throughout a typical day with peak PV output.

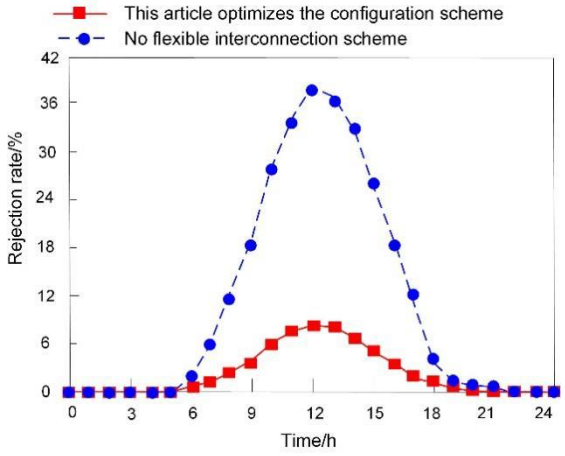

Fig. 3. Comparison curve of light rejection rate at each time of the day

Early Access

This paper has been accepted for publication in the AEE journal. This is the version, which has not been fully edited and content may change prior to final publication.
Citation information: DOI 10.24425/aee.2027.17590

Figure 3 shows that the optimized configuration proposed in this paper yields lower curtailment rates than the non-flexible interconnection scheme across all 24 time slots of a typical day with peak PV output. This is particularly evident during the peak PV output period from 10:00 to 15:00, when the average curtailment rate for the optimized configuration is 6.9%, compared to 32.8% for the non-flexible interconnection scheme. The curtailment rate of the optimized configuration proposed in this paper is, on average, 25.9 percentage points lower than that of the scheme without flexible interconnection. These results validate that the flexible interconnection topology proposed in this paper, through the active power transfer capability of E-SOP, significantly enhances the renewable energy integration level in the new power system of heavy-load regions.

3.3. Verification of safety improvements

By examining the improvements in both system voltage quality and load balancing achieved by the method proposed in this paper, we verify its effectiveness in enhancing system operational safety. The evening peak period (19:00–21:00) was selected for this analysis and verification. During this period, PV output has dropped to zero, load demand reaches its peak, and energy storage systems provide support through discharge; this is a critical period for testing the system's voltage quality and load balancing capabilities. A comparison of voltage distribution at various system nodes and the load factor of transformer districts under the two scenarios—the configuration without flexible interconnection and the optimized configuration proposed in this paper—is shown in Fig. 4. The voltage upper and lower limits are 0.95 p.u. and 1.05 p.u., respectively, and the safe upper limit for the load factor is 80%.

Early Access

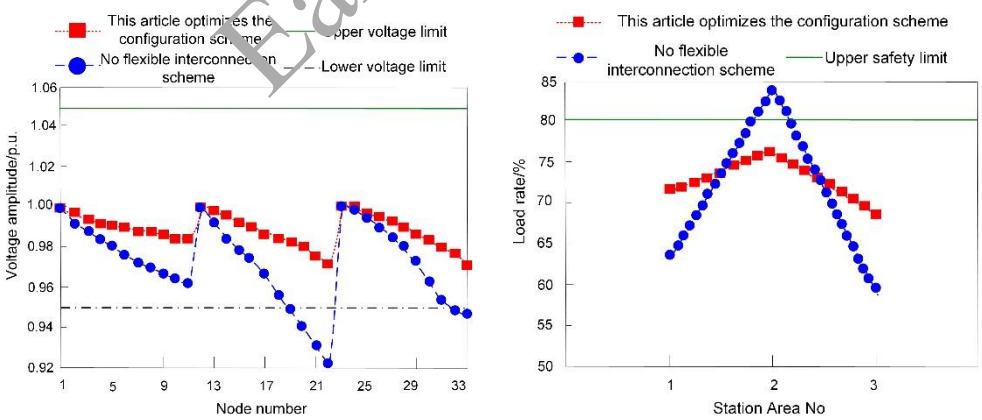

(a) (b)

Fig. 4. Comparison of voltage distribution at each node and load rate in the station area during the evening peak hours (a); Node voltage distribution (b); Station area load rate

This paper has been accepted for publication in the AEE journal. This is the version, which has not been fully edited and content may change prior to final publication.
Citation information: DOI 10.24425/aee.2027.17590

As shown in Fig. 4(a), under the non-flexible interconnection scheme, a total of 7 nodes experienced voltage drops below the lower limit. Among them, the voltage at node 18–22 at the end of Feeder 2 dropped significantly, falling to a minimum of 0.921 p.u., which is below the lower limit requirement of 0.95 p.u. The voltages at nodes 32 and 33 on Feeder 3 were also below the lower limit. Under the optimized configuration proposed in this paper, there are no nodes with voltage exceeding the limit. This is because, under this optimized configuration, the E-SOP supports voltage through reactive power compensation while simultaneously transferring active power from heavily loaded feeders to lightly loaded feeders, enabling all node voltages to be raised to 0.956 p.u. or higher, thereby meeting the system's voltage constraint requirements.

Figure 4(b) shows that under the non-flexible interconnection scheme, the load factor of Substation 2 reaches as high as 84.8%, exceeding the safety threshold of 80% and posing a risk of overload; the load factors of Substations 1 and 3 are 64.2% and 58.7%, respectively, with a variance of 0.0154 among the three substations. Under the optimized configuration proposed in this paper, through active power transfer via the E-SOP, the load factor of Substation 2 is reduced to 76.8%, while those of Substations 1 and 3 increase to 71.3% and 68.5%, respectively. The variance in load factors is reduced to 0.0018, representing a decrease of 88.3%. The above results validate that the flexible interconnection topology proposed in this paper, through the reactive power compensation and active power transfer capabilities of the E-SOP, improves voltage quality and equipment load balancing in the new power system of heavy-load areas.

The reasons for the above voltage and load-rate results are as follows. During the evening peak, PV output is zero and load demand reaches its maximum, so the feeder-end nodes (nodes 18–22 and 32–33) suffer from the largest voltage drop because the reactive power support from conventional capacitors is insufficient. The E-SOP, operating in the VdcQ mode, injects reactive power at nodes 17 and 28, which raises the voltage of the adjacent feeder-end nodes; at the same time, it transfers active power from the heavily loaded Feeder 2 to Feeders 1 and 3, which reduces the current and voltage drop along Feeder 2. For the load rate, the original feeder loads are unevenly distributed, with Substation 2 reaching 84.8%, while Substations 1 and 3 are only 64.2% and 58.7%. The active power transfer of the two E-SOPs redistributes the load among the three station areas, so the load rate of Substation 2 decreases to 76.8% and those of Substations 1 and 3 increase to 71.3% and 68.5%, which explains the 88.3% reduction in load-rate variance.

3.4. Comprehensive comparison of multi-objective optimization configuration schemes

Based on the results of the three sets of experiments described above, the multi-objective optimization configuration scheme proposed in this paper is comprehensively compared with the Puma optimization method, the DG and FCL unit optimization methods, the battery energy storage optimization method, and the stochastic gradient method (methods described in References [8]–[11]).Specifically, the Puma optimization method employs Puma optimization technology to optimize the planning of different types of distributed generation units in a radial distribution network; the DG and FCL unit optimization methods optimize the configuration of distributed generation units and fault current limiter (FCL) units in the distribution network to balance protection coordination and cost reduction; the battery energy storage optimization

Early Access

This paper has been accepted for publication in the AEE journal. This is the version, which has not been fully edited and content may change prior to final publication.
Citation information: DOI 10.24425/aee.2027.17590

method optimizes the configuration of the battery energy storage system to improve system reliability and voltage-frequency stability; the stochastic gradient method employs a stochastic gradient control algorithm to improve power quality in a three-phase distribution system with grid-connected solar photovoltaic generation. The results of the comprehensive comparison are shown in Table 3.

Table 3. Comparison of comprehensive performance of each method

Evaluation index	**Puma optimization method**	**Optimization method of DG and FCL cells**	**Optimization method of battery energy storage**	**Random gradient method**	**Method in this paper**
Power loss after fault/kwh	6.8	8.2	5.4	7.6	2.8
Comprehensive light rejection rate of the system/%	15.3	18.6	12.4	16.8	4.7
Minimum node voltage/p.u	0.931	0.925	0.938	0.928	0.956
Maximum station area load rate/%	84.2	86.5	81.7	85.3	76.8
Load rate variance	0.0086	0.0112	0.0065	0.0098	0.0018
Whether to configure flexible interconnection	No	No	No	No	Yes
Multi objective optimization or not	Yes	Yes	Single target	Single target	Yes

Early Access

As shown in Table 3:

1) Reliability

The post-fault power loss of the method proposed in this paper is 2.8 kWh, representing reductions of 58.8%, 65.9%, 48.1%, and 63.2% compared to the Puma optimization method, the DG and FCL unit optimization methods, the battery energy storage optimization method, and the stochastic gradient method, respectively. This is because the method proposed in this paper uses the E-SOP as the core control mechanism, leveraging its millisecond-level fault-to-supply switching capability to significantly shorten load restoration time, whereas the comparison methods do not incorporate flexible interconnection devices and can only rely on traditional switching operations to restore power supply.

2) Environmental performance

The comprehensive solar curtailment rate of the method proposed in this paper is 4.7%, representing reductions of 69.3%, 74.7%, 62.1%, and 72.0% compared to the Puma optimization

This paper has been accepted for publication in the AEE journal. This is the version, which has not been fully edited and content may change prior to final publication.
Citation information: DOI 10.24425/aee.2027.17590

method, the DG and FCL unit optimization methods, the battery energy storage optimization method, and the stochastic gradient method, respectively. This is attributable to the active power transfer mechanism via the E-SOP, which redirects surplus PV power from lightly loaded feeders to heavily loaded feeders or energy storage devices, thereby enabling cross-feeder coordinated integration of renewable energy.

3) Safety

The minimum node voltage achieved by the method proposed in this paper is 0.956 p.u., the maximum load factor of a feeder section is 76.8%, and the variance of the load factor is as low as 0.0018; all three indicators outperform the comparison methods. This indicates that the method proposed in this paper, through the synergistic effect of reactive power compensation and active power transfer via the E-SOP, possesses significant advantages in improving voltage distribution and balancing feeder loads.

In summary, the method proposed in this paper outperforms four typical configuration methods—the Puma optimization method, the DG and FCL unit optimization methods, the battery energy storage optimization method, and the stochastic gradient method—in terms of reliability, environmental friendliness, and safety. Although the proposed method requires the additional configuration of flexible interconnection devices, the comprehensive performance improvement achieved through multi-objective coordinated optimization is significant, validating the effectiveness of the proposed multi-objective optimization method for flexible interconnection grid topologies in new power systems for heavy-load regions.

Early Access

3.5. Economic assessment and impact of energy-storage operational parameters

To evaluate the economic feasibility of the proposed configuration, the annualized equivalent cost is calculated as the sum of the annualized E-SOP investment, the annual operation and maintenance cost, and the expected outage cost. With a discount rate of 8% and a lifetime of 15 years, the annualized E-SOP investment is about 0.12 MCNY/year, the annual O&M cost is about 0.03 MCNY/year, and the expected outage cost is reduced from 0.41 MCNY/year to 0.05 MCNY/year. The net annual benefit is therefore about 0.21 MCNY/year, and the payback period is about 4.8 years.

The impact of energy-storage operational parameters is further examined. When the daily charge/discharge cycle number increases from 1 to 2, the PV curtailment rate decreases slightly from 4.7% to 4.1%, but the battery equivalent full-cycle life decreases by about 35%. Considering a battery aging cost of 0.15 CNY/kWh per equivalent full cycle, the total annual cost increases by about 18%, which offsets most of the curtailment benefit. Therefore, the recommended operating strategy is one charge/discharge cycle per day with the depth of discharge limited to 80%, which balances the accommodation benefit and battery aging. These results indicate that the proposed method should be accompanied by a battery-degradation-aware dispatch constraint in practical engineering.

These results imply that the superiority of the proposed method mainly comes from the cross-feeder active power transfer capability of the E-SOP rather than from a better single-objective optimizer. The comparison methods either lack flexible interconnection devices or optimize only

This paper has been accepted for publication in the AEE journal. This is the version, which has not been fully edited and content may change prior to final publication.
Citation information: DOI 10.24425/aee.2027.17590

one aspect (e.g., DG siting, FCL coordination, battery storage or reactive power control), so they cannot simultaneously reduce post-fault load loss, PV curtailment and voltage/load-rate deviation. The reason the proposed method achieves the best comprehensive performance is that its three objectives are coupled through the same E-SOP control variables: the active power transfer that reduces curtailment also relieves feeder overload and improves voltage, while the reactive power compensation further reduces voltage deviation. This coupling explains why the proposed method outperforms the four comparison methods in all three dimensions rather than trading one objective against another.

4. Conclusions

In response to the pressures on power supply reliability, renewable energy integration, and operational safety faced by new power systems in heavy-load regions, this paper proposes a multi-objective optimization method for power grid topology configuration centered on flexible interconnection devices (E-SOP) as the core control mechanism. The following conclusions are drawn:

1) The proposed method sets reliability, environmental sustainability, and safety as optimization objectives, with economic feasibility as a boundary constraint. This differs from the traditional approach of optimizing economic and technical indicators in parallel, embodying the engineering logic of "pursuing technical optimality within a limited investment." By establishing a multi-objective model that minimizes load loss, wind and solar curtailment, and the variance of voltage deviation and load factor, the method achieves the coordinated optimization of the new power system's multidimensional performance.

2) This paper validates the method using a case study of a heavy-load region based on the modified IEEE 33-node system. Experimental results show that, in terms of reliability, the E-SOP can complete fault transfer within 0.05 s, reducing the power outage volume by 88.6%; in terms of environmental sustainability, the system's comprehensive solar curtailment rate decreases from 22.6% to 4.7%, a reduction of 79.2%; in terms of safety, the minimum node voltage increased from 0.921 p.u. to 0.956 p.u., and the variance of the load factor decreased by 88.3%. Comparisons with four typical methods—the Puma optimization method, the DG and FCL unit optimization methods, the battery energy storage optimization method, and the stochastic gradient method—further validated the superiority of the method proposed in this paper.

3) The core advantage of the method proposed in this paper lies in the following: Based on the physical capabilities of the E-SOP—active power transfer, reactive power compensation, and fault transfer—it deeply integrates the control mechanisms of flexible interconnection topologies with a multi-objective optimization model, thereby achieving a synergistic improvement in three aspects of the new power system in heavy-load regions: power supply reliability, renewable energy integration, and operational safety. This method provides a theoretical basis and technical

Early Access

This paper has been accepted for publication in the AEE journal. This is the version, which has not been fully edited and content may change prior to final publication.
Citation information: DOI 10.24425/aee.2027.17590

reference for the planning and retrofitting of distribution grids in heavy-load regions under conditions of high renewable energy penetration.

Appendix A. Input data of the test system

The modified IEEE 33-node system operates at 10 kV with a total peak load of 7.2 MW and a PV penetration rate of 45%. The line resistance and reactance are 0.0922 Ω/km and 0.0470 Ω/km, respectively, and the line length of each branch is set according to the original IEEE 33-node system. The PV units are installed at nodes 4, 6, 8, 11, 15 and 28 with capacities of 120, 500, 200, 150, 400 and 600 kW, respectively. The load powers at nodes 17, 22, 26, 31 and 33 are 320, 180, 180, 220 and 140 kW, respectively. The energy storage units have a capacity of 200 kW/400 kWh, a SOC range of 0.1–0.9, and a rated charging/discharging power of 200 kW. The two E-SOPs have a port capacity of 800 kVA each, a power loss coefficient of 2%, and are installed between nodes 8–17 and nodes 19–28, respectively. The time-of-use electricity price is 1.0, 0.7 and 0.4 CNY/kWh for peak, flat and valley periods, respectively.

Early Access

References

[1] Fan P., Yang J., Ke Y.X.L., *Load frequency control strategy for islanded multimicrogrids with v2g dependent on learning-based model predictive control*, IET Generation, Transmission & Distribution, vol. 17, no. 21, pp. 4763–4780 (2023), DOI:10.1049/gtd2.12997.

[2] Qi Z., Peng S., Lim M.K., Tseng M.L., *Photovoltaic storage charging stations considering distribution network sufficiency: a multi-objective capacity optimization allocation*, Journal of Energy Storage, vol. 140, no. Dec. Pt. B, pp. 1.1–1.22 (2025), DOI: 10.1016/j.est.2025. 119096.

[3] Fayez M., Mandor M., El-Hadidy M., Bendary F., *Fuzzy Logic Based Dynamic Braking Scheme for Stabilization of Inte. Area*, Acta Electronica Malaysia, vol. 3, no. 2, pp. 16–22 (2019), DOI: 10.26480/aem.02.2019.16.22.

[4] Zellagui M., Belbachir N., Lasmari A., Molu R.J.J., Kamel S., *Enhancing pv distributed generator planning in medium-voltage dc distribution networks: a multi-design techno-economic analysis with load demand response*, IET Generation, Transmission & Distribution, vol. 18, no. 1, pp. 173–189 (2024), DOI: 10.1049/gtd2.13080.

[5] Sankar M.M., Chatterjee K., *Multi-objective optimal allocation of renewable distributed generation units in a distribution network under high penetration of plug-in hybrid electric vehicles*, Electrical Engineering, vol. 107, no. 5, pp. 6075–6097 (2025), DOI: 10.1007/ s00202-024-02849-z.

[6] Saurav P.K., Mansani S., Kayal P., *Multi-objective planning for optimal location, sizing, and power factor of distributed generators with capacitor banks in unbalanced power distribution networks*, Electrical Engineering, vol. 107, no. 3, pp. 2411–2434 (2025), DOI: 10.1007/ s00202-024-02612-4.

[7] Parsibenehkohal R., Jamil M., Khan A.A., *A multi-stage framework for coordinated scheduling of networked microgrids in active distribution systems with hydrogen refueling and charging stations*, International Journal of Hydrogen Energy, vol. 71, no. Jun., pp. 1442–1455 (2024), DOI: 10.1016/ j.ijhydene.2024.05.364.

[8] Maurya P., Tiwari P., Pratap A., *Puma optimizer technique for optimal planning of different types of distributed generation units in radial distribution network considering different load models*, Electrical Engineering, vol. 107, no. 3, pp. 2777–2828 (2025), DOI: 10.1007/ s00202-024-02631-1.

This paper has been accepted for publication in the AEE journal. This is the version, which has not been fully edited and content may change prior to final publication.
Citation information: DOI 10.24425/aee.2027.17590

[9] Akbar F.A., Reza R., Hesamedin S.S.H., *Optimal allocation and sizing of dg and fcl units in distribution networks to ensure protection coordination and cost reduction*, Electrical Engineering, vol. 106, no. 3, pp. 3243–3252 (2024), DOI: 10.1007/s00202-023-02124-7.
[10] Zhang D., Shafiullah G.M., Das C.K., Wong K.W., *Optimal allocation of battery energy storage systems to improve system reliability and voltage and frequency stability in weak grids*, Applied Energy, vol. 377, no. Jan. 1 Pt. B, pp. 1.1–1.29 (2025), DOI: 10.1016/j.apenergy.2024.124541.
[11] Prasad D., Kumar N., Sharma R., Alotaibi M.A., Malik H., García Márquez F.P., *Stochastic-gradient-based control algorithms for power quality enhancement in solar photovoltaic interfaced three-phase distribution system*, IET Generation, Transmission & Distribution, vol. 18, no. 22, pp. 3567–3578 (2024), DOI: 10.1049/gtd2.13300.
[12] Gorle P.K., Naik R.S., Chappa A., Naidu K.A., Chinta D.P., *Cascade control scheme for frequency control of wind-integrated multi-area multi-machine ac/dc-interlinked power system with deregulation*, Electrical Engineering, vol. 107, no. 7, pp. 9055–9070 (2025), DOI: 10.1007/ s00202-024-02896-6.
[13] Kazma M.H., Taha A.F., *Revisiting the optimal pmu placement problem in multimachine power networks*, IEEE Transactions on Control Systems Technology, vol. 33, no. 2, pp. 493–511 (2025), DOI: 10.1109/TCST.2024. 3487029.
[14] Kim I., *Optimal allocation of distributed generation and storage systems using multi-dimensional weighted least distance optimization and water droplet algorithms*, Energy, vol. 320, no. Apr. 1, pp. 135371.1–135371.11 (2025), DOI: 10.1016/j.energy.2025.135371.
[15] Ran J., Zhang Q., Zhu Y. *et al*., *Co-optimization of thermal-aware workload scheduling with deep reinforcement learning-based cooling control in data centers*, Energy, vol. 344, pp. 139965−139965 (2026), DOI: 10.1016/j.energy.2026.139965.
[16] Asgharzadeh M., Zahedi R., Heidary S., *Energy Modeling: A Comparison of Statistical Methods and Artificial Neural Networks for Electricity Load Forecasting*, 2025 10th International Conference on Technology and Energy Management (ICTEM), IEEE (2025) DOI: 10.1109/ictem66196.2025.11063611.
[17] Vanaja N., Banumalar K., Suresh S., Bhuvanesh A., *Application of fuzzified genetic algorithm for optimal allocation of renewable energy sources into the power system*, Electrical Engineering, vol. 106, no. 6, pp. 6749–6771 (2024), DOI: 10.1007/ s00202-024-02396-7.
[18] Beihropathai V.S., Lalchhandama H., Das P., Kumar C., Chatterjee S., *Optimum solar power usage as an off-grid/on-grid energy-security alternative for the state of Mizoram in India*, Electrical Engineering, vol. 107, no. 7, pp. 9353–9368 (2025), DOI: 10.1007/s00202-025-02976-1.
[19] Karkian E., Askarzadeh A., Alipour M.A., *Uncertainty-based optimal planning of service transformers in distribution network considering load profile: risk-averse and risk-taker strategies modelled by information gap decision theory*, Electrical Engineering, vol. 107, no. 5, pp. 5957–5982 (2025), DOI: 10.1007/s00202-024-02843-5.
[20] Singh K.C., Singh N.P., *An optimized estimation techniques for enhancing the efficiency of power demand in smart grid application*, Wireless Networks, vol. 30, no. 1, pp. 577–591 (2024), DOI: 10.1007/s11276-023-03507-1.
[21] Jagtap K.M., Shukla A., Baboria S.A., *Optimal planning for distribution networks considering system uncertainties using pseudo-inspired gravitational search algorithm*, Electrical Engineering, vol. 107, no. 7, pp. 8569–8588 (2025), DOI: 10.1007/s00202-024-02382-z.
[22] Tashakor N., Kacetl J., Fang J., Li Z., Goetz S., *Generic dynamically reconfigurable battery with integrated auxiliary output and balancing capability*, IEEE Transactions on Power Electronics, vol. 38, no. 7, pp. 7933–7944 (2023), DOI: 10.1109/TPEL.2023. 3263809.
[23] Xu T., Zeng C., *Simulation of Optimization Configuration Algorithm for Energy Storage Capacity in Microgrid*, Computer Simulation, vol. 41, no. 2, pp. 115–119 (2024), DOI: 10.3969/j.issn.1006-9348.2024.02.021.

Early Access